Pulsations Along Stellar Evolution
VIII LAPIS Summer School
AAA Workshop Series 12, 2021
M. Kraus & A.F. Torres, eds.

Pulsating A-F Stars

J. P. Sánchez Arias[1,2]

[1]*Instituto de Astrofísica de La Plata. CONICET-UNLP, Argentina*
[2]*Astronomical Institute, Czech Academy of Sciences, Fričova 298, 251 65 Ondřejov, Czech Republic*

Abstract.

This Chapter provides a brief description of the different classes of pulsating A-F stars emphasising hybrids δ Sct-γ Dor stars. A modelling technique for hybrid δ Sct-γ Dor stars is presented along with the typical features that these stars "print" on their light curves and frequency spectra. Finally, we present a very different family of pulsating stars overlapping the region where pulsating A-F stars usually lie, the precursors of the so-called extremely low mass white dwarf stars. These stars have very similar atmospheric characteristics and their oscillation periods partially overlap making them difficult to discern. We discuss tools based on their seismic oscillation properties to distinguish them.

Key words: asteroseismology — stars: oscillations — stars: interiors

1. The Zoo of Pulsating A-F Stars

There are many families of pulsating stars grouped in different regions of the Hertzsprung-Russel (H-R) diagram. Figure 1 shows schematically some of these families in a seismic H-R diagram. Pulsating A-F stars lie approximately at the lower part of the classical instability strip and its intersection with the Main Sequence (MS) toward temperatures between 6700 and 8500 K. This interesting region of the seismic H-R diagram, harbours a large variety of families and subfamilies of pulsating stars with different physical and pulsational characteristics at different evolutionary stages (pre-MS, MS and post-MS).

Among these families, the best known are: solar-like stars with solar-like oscillations, the rapid oscillators Ap stars, SX Phoenicis stars, λ Boo stars, γ Dor, δ Sct and hybrids δ Sct-γ Dor stars. We will begin this section with a brief description of each of these families.

1.1. Solar-Like Stars With Solar-Like Oscillations

The internal structure of these stars is similar to the Sun, they have a radiative core with a large convective envelope. In general, stellar pulsations can be classified according to their driving mechanism in self-excited oscillations and stochastic oscillations. Self-excited oscillations arise from a perturbation of the energy flux resulting in a heat-engine mechanism. If the variation is in the opacity, we have the κ-mechanism; if the variation cames from the temperature rising

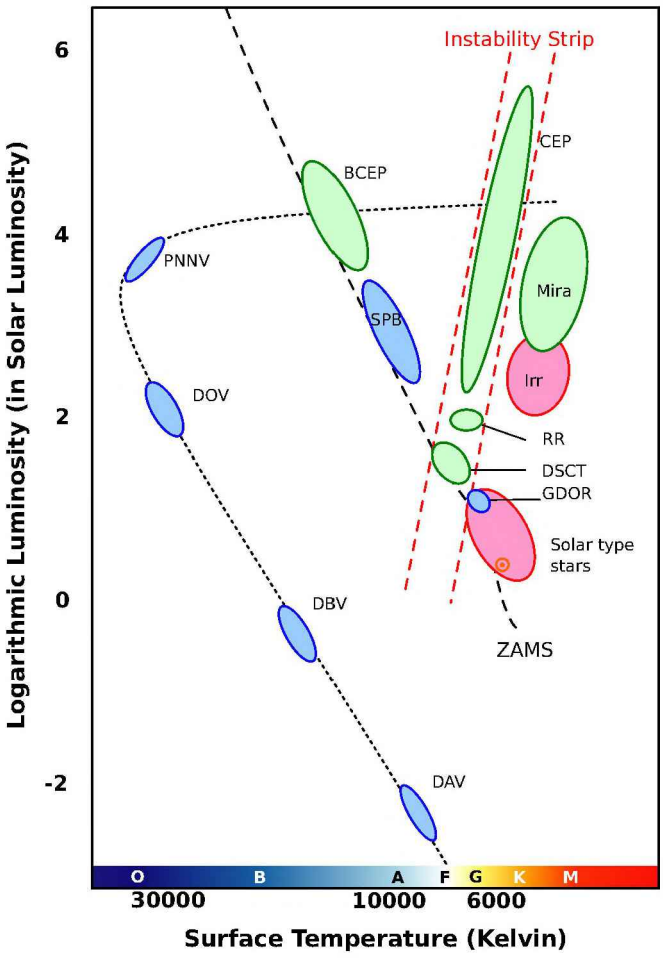

Figure 1. Seismic H-R diagram showing different families of pulsating stars. The classical instability strip is indicated in red lines, the beginning of the MS in black dashed line and the cooling track in black dotted line.

from nuclear reactions, then the operating mechanism is the ϵ-mechanism. On the other hand, stochastic oscillations are excited and damped usually by turbulent convection. Solar-like oscillations are driven stochastically and are expected to be present in all stars with outer convective zones.

1.2. Rapidly Oscillating Ap Stars

Rapidly Oscillating Ap (RoAp) stars belong to Population I. They have a particular chemical surface composition caused by atomic diffusion (specifically due to the effect of gravitational settling and radiative levitation). One of their main characteristics is their strong magnetic field. In addition, they usually present spots and stratification (Aerts et al., 2010). Their oscillation periods are between ~ 4.7 and 21 min and they correspond to high radial order, low degree pressure modes (or p-modes).

1.3. SX Phoenicis Stars

These stars belong to Population II and are characterised by low metallicities between 0.002 and 0.0002. SX Phoenicis (SX Phe) stars have masses in the range 0.9 to 1.15 $M_{\odot}$ and oscillations very similar to those of δ Sct stars. They are thought to be blue straggler stars, i.e. MS stars in a open or globular cluster that are more luminous and bluer than stars at the MS turnoff point for the cluster. One possible explanation for this behaviour lies in mass transfer between two stars born in a binary star system. The more massive star will evolve first and as it expands, will overflow its Roche lobe. Then mass will quickly transfer from the initially more massive companion on to the less massive one and this would explain why there would be MS stars more massive than other stars in the cluster which have already evolved off the MS.

1.4. λ Boo Stars

This family of pulsating A-F stars, consists of Population I stars with a superficial chemical impoverishment possibly due to the accretion of metal deficient gas in the circumstellar environment. Recent studies indicate that not all λ Boo stars are young and are found at a variety of MS ages (Murphy et al., 2020). Their oscillations are similar to δ Sct stars.

1.5. δ Sct Stars

One of the most representative group of pulsating A-F stars are δ Sct stars. They can be found on the MS and pre-MS with masses usually between 1.5 and 2.5 $M_{\odot}$. They oscillate in non-radial p-modes of low to intermediate radial order, and also show radial modes, with periods usually between 0.008 and 0.42 days which allow to probe the external layers of the star. These oscillations are driven mainly by the κ-mechanism operating in the partial ionisation He layer and the turbulent pressure acting in the H ionisation zone (Antoci et al., 2014). Their internal structure is characterised by a convective core surrounded by a radiative layer with a thin outer convective layer. In the Sun, this layer encompasses approximately 30% of the Sun, while in δ Sct stars this layer encompasses $\sim 1\%$.

1.6. γ Dor Stars

Another important group among pulsating A-F stars is formed by γ Dor stars. These stars are found in pre-MS, MS and post-MS. In general, they are less massive than δ Sct stars, with masses between 1.5 and 1.8 $M_{\odot}$ and effective temperatures between 6700 K and 7500 K. They pulsate in high radial order gravity-modes (or g-modes) with periods around 8 hrs and 3 d driven by the convective blocking mechanism. In γ Dor stars, the convective envelope is thought to be deeply enough to reach the layer where the κ-mechanism usually operates, i.e. the ionisation He II layer. The heat flux is then conducted by convection and the κ-mechanism is suppressed. The presence of g-modes in these stars allows us to probe the near-to-core layers.

1.7. Hybrid δ Sct-γ Dor Stars

These stars pulsate in many radial and non-radial p- and g-modes which makes them excellent targets for asteroseismology. The simultaneous presence of p- and g- modes allows to explore their external layers as well as the near-to-core layers, respectively. A typical light curve of this kind of stars often shows two separate ranges of frequencies: one corresponding to high frequencies characteristic of δ Sct (p-modes) and the other one at low frequencies usually characteristic of γ Dor (g-modes) (see Section 2.1). They usually lie in the overlapping instability region of δ Sct and γ Dor stars. However, the advance of space missions opened new interrogations due to the interesting results of such observations. For instance, several new hybrid δ Sct-γ Dor stars were found thanks to these missions and some of them lie outside their predicted instability strip. Moreover, the same is true for δ Sct and γ Dor stars. These observations showed that hybrid δ Sct-γ Dor stars are more common than expected and also made us wonder about the intrinsic characteristics of δ Sct, γ Dor, and hybrid stars, along with the driving mechanisms operating in these stars. It is believed that both mechanisms operate in hybrid stars: the κ-mechanism and the convective blocking mechanism, but up to date these have not been further analyzed.

2. Asteroseismology of Hybrid δ Sct- γ Dor Stars

As we mentioned before, asteroseismology is a magnificent tool which allows us to obtain valuable information about the interior variable stars and the physical processes that take place inside them. The main aims of asteroseismic modelling of stars are to get high precision in astrophysical parameters such as the mass (M), the radius (R) and the age; and to improve input physics of the stars by means of a comparison between theory and observations. The input physics of the target object is first adjusted to derive a stellar model and theoretical predictions for oscillations. Then, these predictions are compared to the observed properties of identified oscillation modes through photometric, spectroscopic and/or astrometric observations.

Next, we will see the features commonly found in the light curves of hybrid δ Sct-γ Dor stars and we will review the main steps for a particular kind of modelling of these stars.

2.1. Light Curves and Frequency Analysis of Hybrid δ Sct-γ Dor Stars

In this section, we will introduce the main features usually present in the frequency spectra of hybrid δ Sct-γ Dor stars as well as some corrections that usually have to be made in the light curves, specially for those provided by the COnvection ROtation et Transits planétaires (CoRoT) CNES/ESA space mission (Auvergne et al., 2009) before we can perform the frequency analysis. This space mission was launched in 2006 and offers five observing runs with durations of 59, 28, 157, 148 and 20 days with different integration time: 1, 32 and 512 s.

One of the phenomena that usually affect light curves and should be inspected before performing the frequency analysis is the impact of cosmic rays. These impacts lead to individual outlier measurements that should be removed before the frequency analysis. Another phenomenon we have to take into account for CoRoT light curves is that they usually have a slope which translates into frequencies below 0.25 c/d (Chapellier & Mathias, 2013). These frequecies must not be taken into account during the frequency analysis. Finally, it is important to remove the rotational frequency of the satellite ($f_{orb} = 13.97213\, c/d$) and its harmonics ($n * f_{orb}$), in order to employ only pulsational frequencies during the modelling.

Let us consider as example the star CoRoT ID 102358531 observed during the third CoRoT long run, LRa03, which targeted the Anti-Galactic center. According to the EXODAT database (Deleuil et al., 2009) this star has $\alpha =$ 6h12m29.58s, $\delta = +4°58'54.2244''$, it has an A0V spectral type and 2MASS photometry $J = 13.363$, $H = 13.191$ and $K = 13.085$. In Figure 2 we show the resulting light curve of CoRoT ID 102358531. This light curve clearly shows a hybrid nature for this star, since it displays both low and high frequency components corresponding to the γ Dor and δ Sct domains, respectively.

After cleaning the light curve we are in conditions to derive the frequency spectrum yielded by the Fourier transform in order to obtain the individual frequencies. As expected, the resulting frequencies from light curves of hybrid δ Sct-γ Dor stars, are usually grouped within two different domains: one corresponding to low frequencies typically related to γ Dor stars, and another domain at higher frequencies typically associated with δ Sct stars. In Figure 3 we show these two groups in the frequencies spectrum of CoRoT 102358531.

Once we obtained the individual frequencies, the search of pattern begins with the aim to identify each frequency and to perform later an asteroseismic modelling. There are different kinds of patterns to look for during the frequency analysis of hybrid stars. We will mention here the mean period spacing of g-modes and rotational splittings.

As we mentioned before, hybrid δ Sct-γ Dor stars oscillate in high order g-modes. According to the asymptotic theory (Tassoul, 1980) the difference between the periods of two consecutive radial order modes with the same harmonic degree (ℓ) tends to be constant for higher radial order modes. Therefore, if we find consecutive equidistant periods in the γ Dor range, these will probably correspond to an asymptotic ($n >> \ell$) series of g-modes with the same ℓ and high radial order. These series will allow us to derive later the mean period spacing of g-modes (if the series has n periods, Π_i, equally separated, then the mean period spacing is $(\Pi_n - \Pi_1)/(n-1)$). This quantity is extremely useful for the

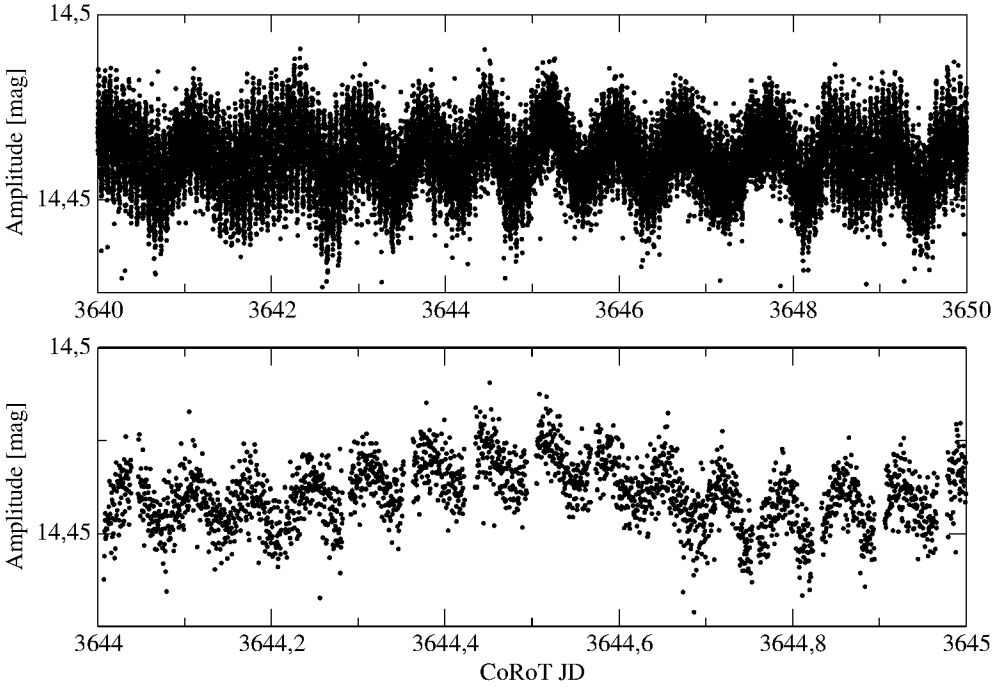

Figure 2. Light curve of the star CoRoT 102358531 with different timescales, a subset over 10 d at the top and a zoom into one day subset at the bottom.

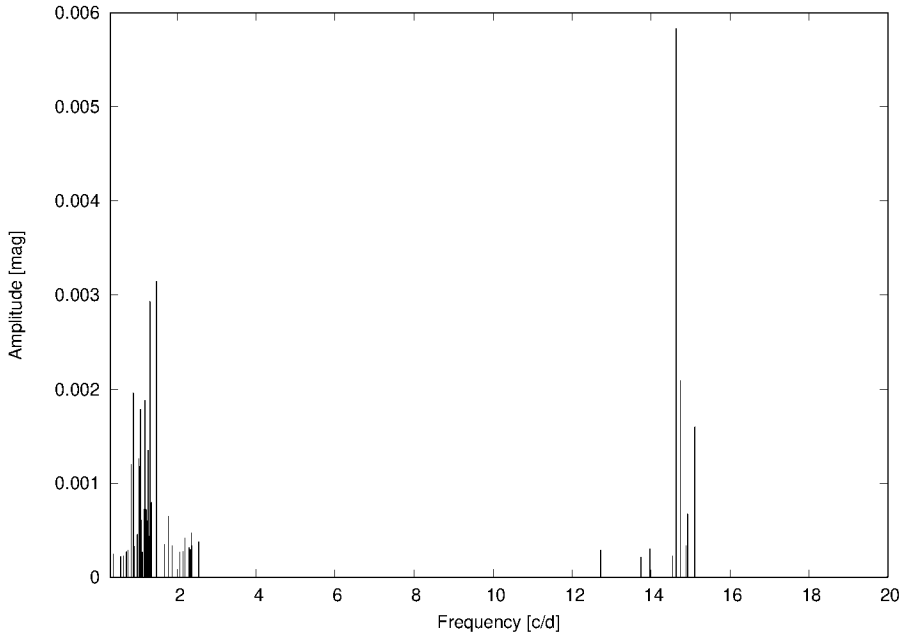

Figure 3. The resulting frequencies and their corresponding amplitudes in CoRoT 102358531. Two different domains are distinguished for this hybrid δ Sct- γ Dor star.

study of hybrid δ Sct-γ Dor stars since it can be employed as an indicator of the evolutionary stages of these stars.

The asymptotic period spacing for g-modes can be written in terms of the Brunt-Väisälä frequency (N):

$$\Delta\Pi_l^a = \frac{2\pi^2}{\sqrt{l(l+1)}} \left[\int_a^b \frac{N}{r} dr \right]^{-1} \tag{1}$$

where a and b are the inner and outer boundaries of the propagation zone of g-modes, respectively. As stars evolve on the MS and consume the H in the core, the Brunt-Väisälä (B-V) frequency, which governs the behaviour of g-modes, is affected by the change of the convective core. For masses greater than $\sim 1.5 M_\odot$, the core shrinks as the star evolves and its edge moves inward. In the case of hybrid stars, the propagation region of g-modes belongs to the inner region of the star and the lower boundary of this region begins immediately after the edge of the convective core. Therefore, during the evolution, the integral increases since it expands toward inner regions resulting in a decreasing asymptotic period spacing of g-modes and therefore a decreasing mean period spacing. This allows us to employ the mean period spacing, usually detected in hybrid stars, to place restrictions for the modelling of these stars.

Another extremely useful patterns that should be investigated during the frequency analysis of these objects are rotational splittings. Pulsating A-F stars are intermediate to fast rotators. In rotating stars, modes can be separated into several components forming multiplets. Considering rigid rotation and the first order perturbation theory, the components of the rotational multiplets are given by:

$$\nu_{nlm} = \nu_{nl} + m(1 - C_{nl}) \frac{\Omega}{2\pi} \tag{2}$$

where ν_{ln} is the central mode of the multiplet, C_{nl} is the Ledoux constant and $\Omega/2\pi$ is the rotational frequency of the star. The Ledoux constant tends to zero for p-modes with an increase in the radial order and tends to $1/(\ell(\ell+1))$ for g-modes. For instance, if we find in the δ Sct regime, the next frequencies series: $\nu_{nl} - f$, ν_{nl}, $\nu_{nl} + f$ they might correspond to a triplet ($\ell = 1$) and we would be able to derive the rotational velocity.

This information along with any other information we can obtain through other methods such as spectroscopy and astrometry should be employed in the theoretical modelling of stars. Next subsection will be devoted to the modelling of hybrid δ Sct-γ Dor stars.

2.2. Modelling Hybrid δ Sct-γ Dor Stars

There are different ways to perform a modelling of a star. In this subsection we will describe a classical grid-based modelling applied to hybrid δ Sct-γ Dor stars based on statistic searches. This procedure is fully described in Sánchez Arias et al. (2017) along with its application to 5 hybrid stars.

The first step in the modelling of stellar interiors is to select a suitable code to create the models. There are several codes to compute stellar structure and pulsational models. Among the best known codes to develop stellar interior

structure models we can mention MESA (Paxton et al., 2011), CESAM2k (Morel & Lebreton, 2008) and LPCODE (Althaus et al., 2005). The first two mentioned codes allow the development of stellar interior models for a wide range of masses at different evolutionary stages including also different physical phenomena such as rotation, different theories of convection and diffusion of chemical elements, among others. On the other hand, LPCODE was fully developed at La Plata Observatory and is also widely employed to simulate the evolution of low-mass stars, mainly, at different stages. This code is coupled to an oscillation code named LP-PUL(Córsico et al., 2006) which allows computing adiabatic oscillation and those which take into account the excitation mechanism, i.e. non-adiabatic oscillations. Apart from LP-PUL, we can mention ADIPLS (Christensen-Dalsgaard, 2008) and GYRE (Townsend & Teitler, 2013) among the best-known oscillation codes. Both codes allow the calculation of adiabatic oscillations and the latter also calculate non-adiabatic oscillations.

Once we have selected a suitable code, we must set the input physics for the target object in order to obtain representative models. The main ingredients to be set are the nuclear reaction network, the opacity tables, the equation of state, a theory for the mixing of elements, a theory for stellar rotation if any, to decide which and how extra mixing process are going to be included, which kind of oscillations we want to study, etc. The input physics should be carefully selected, since the output model strongly depends on it, obviously. We encourage the reader to look for the details of the input physics in Sanchez Arias et al. (2017) and we will focus here in the steps of a particular modelling technique applied to the hybrid δSct-γ Dor stars.

The procedure we will describe next is a grid-based modelling consisting of a statistic search of the model which best fits the observations in a previously constructed grid of representative models of hybrid δ Sct-γ Dor stars. After having carefully selected the input physics in the code, the next step is to construct a grid of representative models. In Figure 4 we can see the location of a sample of δ Sct (open circles), γ Dor (grey squares), and hybrid δ Sct-γ Dor (red star symbols) stars taken from Grigahcène et al. (2010) in an H-R diagram. The grid should fully cover the region where hybrid δ Sct-γ Dor stars usually lie in the H-R diagram in order to employ it for different targets. Precisely, with the aim to encompass these objects with our models, we varied different parameters in our grid such as the mass ($1.2 \leq M_\star/M_\odot \leq 2.2$), the metallicity ($0.01 \leq Z \leq 0.02$), the overshooting[1] parameter ($0 \leq f \leq 0.03$) at different evolutionary stages from the Zero Age Main Sequence (ZAMS) to the Terminal Age Main Sequence (TAMS).

For each evolutionary sequence, we recorded the stellar structure model every 10 K approximately and we computed for them the adiabatic oscillations, specifically we calculated radial modes as well as non radial p- and g-modes with harmonic degree of 1, 2 and 3 with periods between 1200 s and 300000 s encompassing widely the usual periods of the modes found in these stars. Some of the evolutionary sequences of this grid are shown in Figure 4. Those corresponding

[1]Overshooting is the mixing of chemical elements beyond the formal convective boundary set by the Schwarzschild criterion. This phenomenon extends the evolutionary tracks during the evolution on the MS since extra mixing adds more H to the core to be burnt.

to a metallicity of 0.01 with an overshooting parameter of 0.03 are depicted in cyan; while those in black correspond to a metallicity of 0.015 and no overshooting, for different masses indicated with black numbers. It can be seen that the models of the grid encompass the occupied region by these observed stars.

Once we have a grid of representative models for the kind of object we want to study, we are able to perform a search for the model that best reproduces the observations of a given target star. The usually procedure in this grid-based modelling is to calculate a "quality function" for each model. This quality function compares observationally derived quantities with those calculated from the models. This function should reflect the nature of the objects we want to model, which in this case are hybrid δ Sct-γ Dor stars. For instance, hybrid stars oscillate in high order g-modes (as γ Dor stars) and low- to intermediate-order p-modes (as δ Sct stars). As we mentioned before (Section 2.1) it is possible to recognise high order g-mode features during the frequency analysis and employ that pattern as a constraint in the search of the best model. Therefore, including this pattern (or the mean period spacing) in the quality function of hybrid δ Sct-γ Dor stars, along with the information of the individual frequency p- and g-modes, boost this search efficiency.

As an example of the modelling of hybrid stars, we show the application of this procedure for HD 49343 as it was performed in Sánchez Arias et al. (2017). This star was previously studied in Brunsden et al. (2015). We used the information about the individual periods in the γ Dor range ([28800-288000]s), as well as in the δ Sct range ([1080-28800]s) and the observed mean period spacing of g-modes ($\overline{\Delta\Pi} = 2030.4s$) to create the "quality function".

First we calculated the mean period spacing of g-modes for each model. In Figure 5 we show the mean period spacing of g-modes calculated in the range of the observed g-mode periods, for those models of the grid with $Z = 0.01$ and $f = 0.01$ as an example. Each curve corresponds to certain mass and models in the ZAMS have higher mean period spacings (see Section 2.1). As already mentioned, the mean period spacing of g-modes decreases with the evolution. Therefore, this quantity can be used as an indicator of the evolutionary stage of hybrid δ Sct-γ Dor stars. After calculating this quantity, we selected for each $M_\star$, Z and f, the model which best reproduces the mean period spacing of g-modes derived from observations, i.e. those models closer to the straight line in Figure 5.

Next, for the models selected in the previous step we performed a period-to-period fit of p-modes as well as of g-modes, including this information in the quality function. The resulting quality function is:

$$F = \sum_{j=1}^{N} \frac{[\overline{\Delta\Pi_n} - \overline{\Delta\Pi}]_j^2}{(\sigma^2_{\overline{\Delta\Pi}})_j} + \chi_j^p + \chi_j^g, \tag{3}$$

where $\overline{\Delta\Pi_n}$ is the calculated mean period spacing that best reproduces the observed one ($\overline{\Delta\Pi}$) for a certain Z, $M_\star$ and f, $\sigma_{\overline{\Delta\Pi}}$ is the error corresponding to the observed mean period spacing, χ_j^p is the sum of the difference between the periods of p-modes calculated for each model and the period observed in the δ Sct range divided by the error corresponding to the observed frequency; and χ_j^g is the same for individual g-modes. This quality function has its own peculiar-

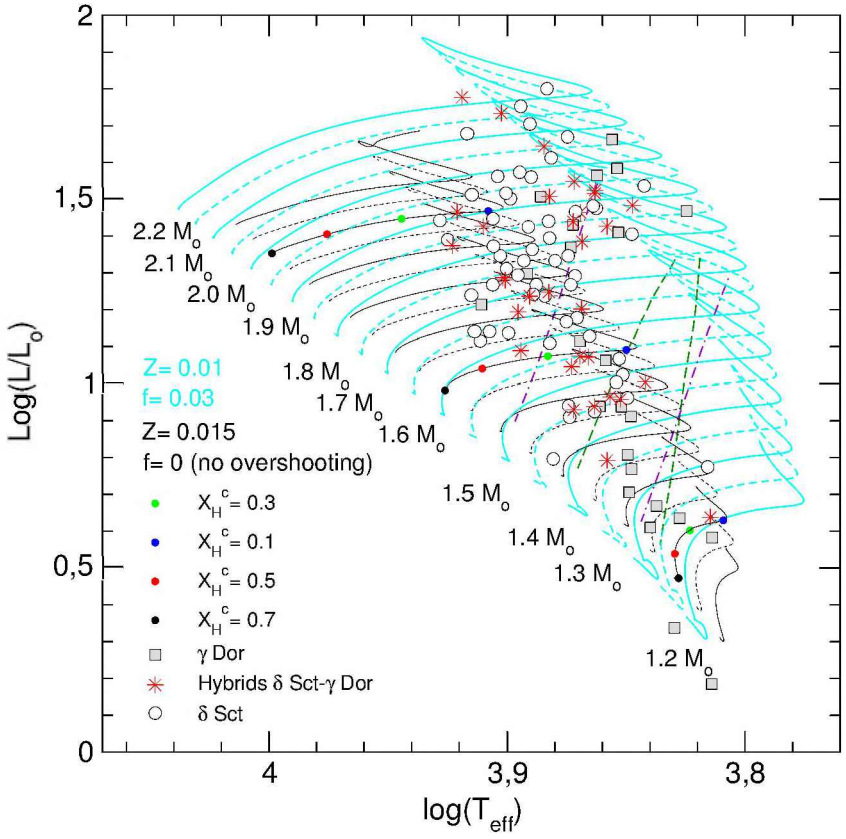

Figure 4. HR diagram showing evolutionary tracks for stellar models with different masses ($1.2M_{\odot} \leq M_{*} \leq 2.2M_{\odot}$), $Z = 0.015$ and without overshooting ($f = 0$) in black, and $Z = 0.01$ and $f = 0.03$ in light blue, from ZAMS to TAMS. The value of the stellar mass ($M_{\star}$) is indicated for a subset of tracks (those displayed in solid lines). Black, red, green, and blue dots correspond to the location of stellar models with $M_{\star}/M_{\odot} = 1.3, 1.7$ and 2.1 having a central H abundance of $X_H^c = 0.7, 0.5, 0.3, 0.1$, respectively. A sample of δ Sct (open circles), γ Dor (grey squares), and hybrid δ Sct-γ Dor (red star symbols) stars taken from Grigahcène et al. (2010) are included for illustrative purposes. Also, the boundaries of the δ Sct (violet dot-dashed lines) and γ Dor (green dashed lines) theoretical instability strips from Dupret et al. (2005) are plotted. Extracted from Sánchez Arias et al. (2017).

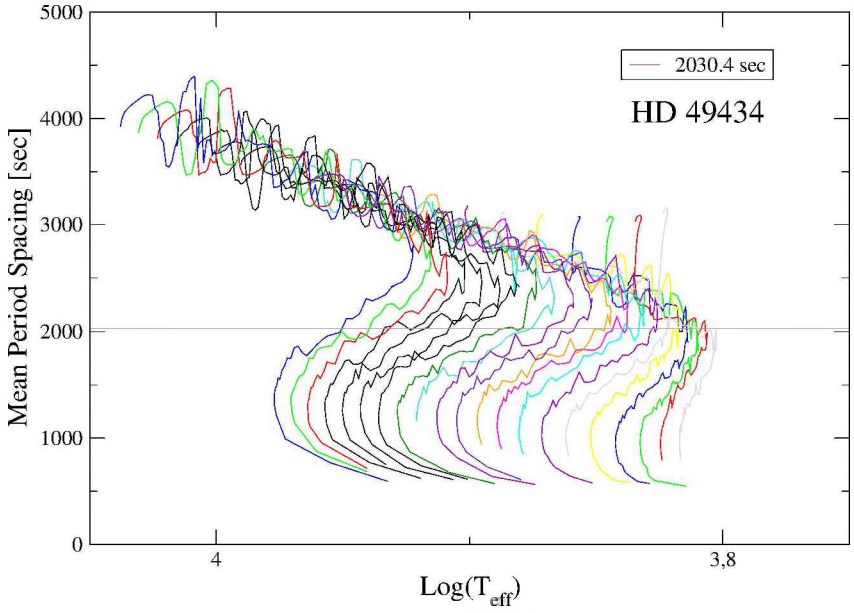

Figure 5. Mean period spacing vs. effective temperature for grid models calculated with $Z = 0.01$ and $f = 0.01$. The straight line represents the observed mean period spacing for g-modes calculated from observations of HD 49434. Extracted from Sánchez Arias et al. (2017).

ities depending on the observed star. For instance, if the harmonic degree was determined for a certain mode, this quality function can be properly adjusted in order to reflect this information, as it has been performed in Sánchez Arias et al. (2017) for every considered star.

Finally, we search for the model with the minimum quality function, which will be the model that best reproduces the observed frequency spectrum of the star.

As it has been mentioned, this is only one way to perform an asteroseismic modelling based on a grid of models. There are several ways to search for a representative model, for instance you can perform a similar search including more information in the quality function such as spectroscopic data.

As a result of the modelling, we obtain valuable information about our object. For example, in the case of HD 49434, we derived the next astrophysical parameters: $M_* = 1.75 M_\odot$, $Z = 0.01$, $f = 0.01$, $T_{eff} = 7399K$, $\log g = 3.85$, $R_{star} = 2.57 R_\odot$, $Age = 1169.08 \times 10^6 yr$, $L_* = 19.39 L_\odot$ and $\overline{\Delta\Pi} = 2045.42s$.

3. Comparing the Asteroseismic Properties of Pulsating Pre-extremely Low Mass White Dwarf and δ Scuti Stars.

There are several problems that can be addressed with asteroseismology. The problem we will focus on in this section concerns the distinction between two very different families of pulsating stars, which have similar atmospherics parameters (T_{eff} and $\log g$).

Thanks to the advance of space missions, new kinds of families started to be discovered. The family of variable stars we are interested in, are the precursors of the so-called the extremely low mass white dwarf stars or pre-ELMV. Extremely low mass white dwarf (ELM) stars (or low mass He-core white dwarfs) are the result of a strong mass transfer event at the red giant stage of low mass star evolution in close binary system. Their masses are below 0.3 solar masses and they oscillate in p- and g-modes driven by the κ-mechanism operating in the second He ionisation zone with periods between 380 and 3500 s approximately. The precursors of these white dwarf stars lie before the cooling sequence of ELM white dwarfs, in the region where pulsating A-F stars usually are (see Figure 6). This is one of the reasons that makes them difficult to distinguish from some pulsating A-F stars, specially δ Sct stars, as we will see next. The correct distinction between these types of pulsating stars will help to discover new members for pre-ELMV white dwarfs and to understand the formation channels for this new family of pulsating white dwarf stars.

In Sánchez Arias et al. (2018) we provided asteroseismic tools in order to distinguish between these two different families, the δ Sct stars and pre-ELMV white dwarf stars. Here we will present a brief resume on such tools aimed to highlight the power of asteroseismology.

Figure 6 shows the position in the HR diagram of δ Sct stars in white circles from Uytterhoeven et al. (2011), Bradley et al. (2015) and Bowman et al. (2016). SX Phe stars are those from Balona & Nemec (2012) depicted in magenta circles. With blue diamonds we show the position of the known pre-ELMVs (Maxted et al., 2013, 2014; Gianninas et al., 2016), while the ELMVs are depicted with light green triangles (Hermes et al., 2012, 2013a,b; Kilic et al., 2015; Bell

et al., 2017). It is also displayed the position of the pulsating object J0757+1448 reported for the first time in Sánchez Arias et al. (2018) with a cyan diamond and the cyan squares indicate the position of two stars reported by Corti et al. (2016), J1730+0706 and J1458+0707. These three stars lie in our region of interest where pre-ELMV stars can be confused with δ Sct star. The nature of these objects was discussed in the previously mentioned paper. We have also included theoretical evolutionary tracks for low mass He-core WD from Althaus et al. (2013) (dotted black lines) and Serenelli et al. (2001) (dashed black lines). Black numbers correspond to the values of the stellar mass of low mass He-core WD evolutionary tracks. In the same figure we illustrate MS evolutionary tracks (with red lines), for different values of metallicity (Z), mass ($M_\star$) and overshooting parameter (f) from Sánchez Arias et al. (2017). Besides, we included the location of the theoretical blue edge and the empirical red edge of the δ Sct instability strip from Pamyatnykh (1999), and also the blue edge of the pre-ELMV instability strip (Córsico et al., 2016).

From this figure, we can see that the theoretical evolutionary sequences of pre-ELMV stars partially overlap with those corresponding to MS stars and the region where pre-ELMVs can lie partially overlaps with the region occupied by the δ Sct stars. Besides, we note that both instability strips overlap for $3 \leq \log g \leq 4.4$. In summary, pre-ELMV and δ Sct stars have very similar atmospheric parameters T_{eff} and $\log g$, their evolutionary sequences partially overlap as well as their instability strips. In addition, both families show an overlapping range of pulsating periods (see Figure 7). Therefore, some pre-ELMV stars might be polluting the region where δ Sct usually lie. With the aim to provide tools to discover more interesting pre-ELMV stars, and distinguish them from δ Sct stars, we analysed and compared theoretical models of their structure and oscillations. The selected models are represented in orange triangles in Figure 6.

Although both kinds of families have the previously mentioned similarities, pre-ELMV and δ Sct stars are at very different stages of their evolution and their internal structure is different. For instance, δ Sct stars have radii between 1.5 and 3.5 $R_\odot$ while pre-ELMV stars with the same $\log g$ have $\sim 0.6\,R_\odot$ and the density for δ Sct stars are much lower than for pre-ELMV white dwarf stars. This fact is of course reflected in their pulsational behaviour, therefore employing only asteroseismology should allow us to distinguish between these kind of stars despite their similar atmospheric parameters.

In order to do this, in Sánchez Arias et al. (2018) we selected, as we mentioned, two sets of models of each type of family in different regions of the H-R diagram in which these families can be incorrectly classified, and we measured the period differences at different ranges of mode periods for each type of stars. Specifically we found that the mean period difference of p-modes of consecutive radial orders for δ Sct model is at least four times larger than the mean period spacing (or the mean period difference of g-modes of consecutive radial order) for the pre-ELMV white dwarf model in the period range $[2000 - 4600]$ s. Therefore, if we detect two periods and we calculate their differences, assuming they have consecutive radial order, we can say whether the star belongs to the pre-ELMV family or to the δ Sct star family according to the obtained value. However, mode

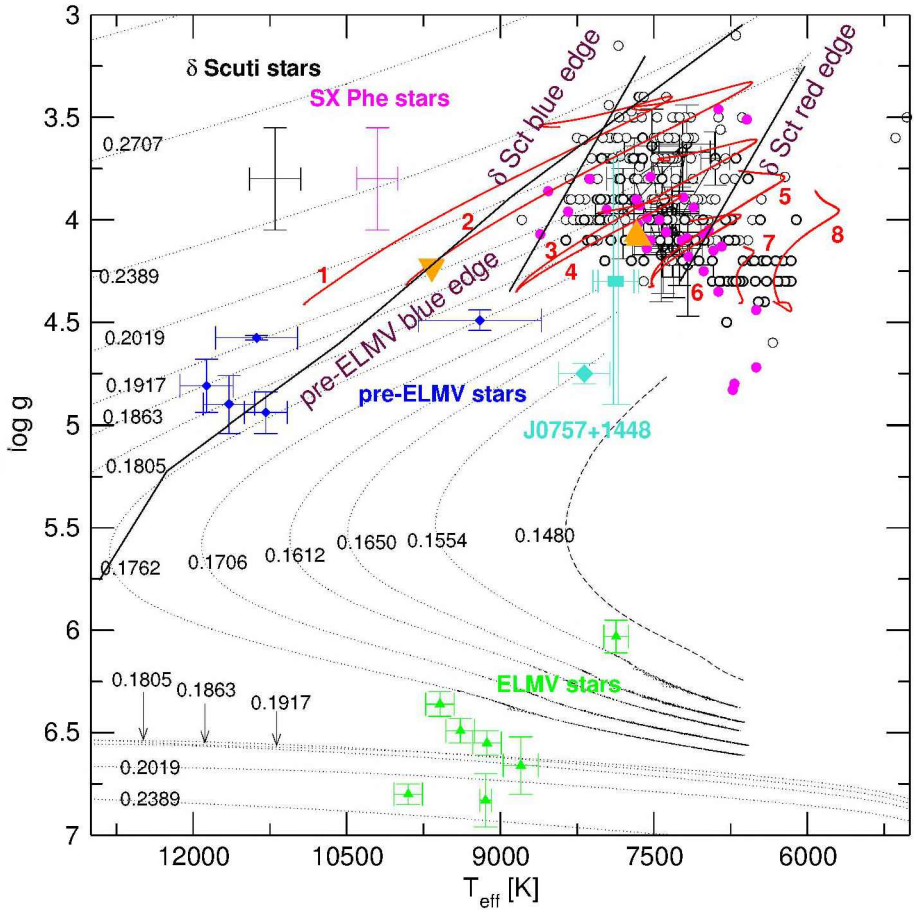

Figure 6. $T_{eff} - \log g$ diagram showing the location of ELMV stars (light green triangles), pre-ELMV stars (blue diamonds) and δ Sct stars (white circles) including SX Phe stars (magenta circles). The atmospheric parameters are extracted from different papers detailed in the main text. The error bars for the δ Sct and the SX Phe stars are depicted in black and magenta respectively. Also, we included the theoretical evolutionary tracks of low mass He-core WDs (black dotted and dashed lines) from Althaus et al. (2013) and Serenelli et al. (2001), and MS evolutionary tracks (red lines) from Sánchez Arias et al. (2017). Black numbers correspond to different values of the stellar mass of low mass He-core WDs, whereas red numbers are associated to the value of the mass, metallicity and overshooting parameter of MS stars. It is also shown the location of the theoretical blue edge and the empirical red edge of δ Sct instability strip from Pamyatnykh (1999), and also the blue edge of the pre-ELMV instability strip (Córsico et al., 2016). Orange triangles show the position of the template models. The cyan squares indicate the position of J1730+0706 and J1458+0707, and the cyan diamond represents the position of J0757+1448. Figure extracted from Sánchez Arias et al. (2018).

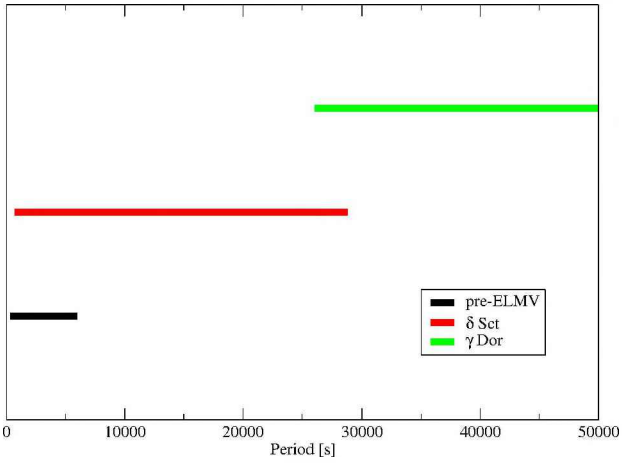

Figure 7. Scheme showing the usually ranges of the observed modes periods for pre-ELMV in black, δ Sct in red and γ Dor stars in green. The γ Dor range extends up to $\sim$260000 s.

identification is not an easy task and in general we cannot verify the hypothesis of consecutive radial order for the observed periods.

Therefore, we can employ another tool which does not depend on mode classification: the rate of period change. As stars evolve their structure changes, therefore their frequencies will also change since they depend on the stellar structure. On the MS the periods change slowly as the stars burn H in their core, while in the stages prior to the cooling sequence of white dwarf stars, they spend just a few years crossing the HR diagram very quickly. Therefore the rate of period change of δ Sct stars and pulsating pre-ELM white dwarf stars should be very different. This is exactly what we found in our models. The predicted rate of period change in δ Sct stars is $\frac{dP}{dt} \approx 5.45 \times 10^{-5}$ s/yr, and for pre-ELMV WD stars is $\frac{dP}{dt} \approx -1.42 \times 10^{-3}$ s/yr. Therefore, this difference allows us to distinguish between these two kinds of families without mode identification and is based only on the oscillation properties of these stars.

4. Summary

In this Chapter we briefly characterised pulsating A-F stars. The differences present between each family belonging to this interesting group allow us to investigate different physical phenomena such as the differential rotation, magnetic field, conservation of angular transport and excitation mechanisms in low mass stars at the pre-MS, MS and post-MS phases.

We focused on hybrid δ Sct-γ Dor stars since the simultaneous presence of p- and g- modes allows us to probe their internal layers as well as their external regions turning them into excellent targets for asteroseismology. We have introduced the main characteristics in the light curves of these objects, along with some of the most useful features in the frequency spectra we should recognise to

perform a modelling of the star. Furthermore, we briefly described one method to perform a grid-based modelling of hybrids δ Sct-γ Dor.

Finally we introduced a very different family of pulsating stars, pre-ELMV white dwarf stars, which lie very close to pulsating A-F stars and might be polluting the region where δ Sct stars usually lie. We showed how asteroseismology can be employed to distinguish them and we presented two different asteroseismic tools to achieve this goal in order to discover new interesting pulsating pre-ELM white dwarf stars.

Acknowledgments. I am very grateful to the organisers for letting me participate as a lecturer in this school and for their work organising an excellent LAPIS School 2019. I would like to thank CONICET for the postdoctoral Fellowship during which this proceeding was partially written. This project has received funding from the European Union's Framework Programme for Research and Innovation Horizon 2020 (2014-2020) under the Marie Skłodowska-Curie Grant Agreement No. 823734.

References

Aerts C., Christensen-Dalsgaard J., Kurtz D. W., 2010, *Asteroseismology*

Althaus L. G., Miller Bertolami M. M., Córsico A. H., 2013, *A&A*, **557**, A19

Althaus L. G., Serenelli A. M., Panei J. A., Córsico A. H., García-Berro E., Scóccola C. G., 2005, *A&A*, **435**, 631

Antoci V., Cunha M., Houdek G., Kjeldsen H., Trampedach R., Handler G., Lüftinger T., Arentoft T., Murphy S., 2014, *ApJ*, **796(2)**, 118

Auvergne M., Bodin P., Boisnard L., Buey J.-T., Chaintreuil S., Epstein G., Jouret M., Lam-Trong T., Levacher P., Magnan A., Perez R., Plasson P., Plesseria J., Peter G., Steller M., Tiphène D., Baglin A., Agogué P., Appourchaux T., Barbet D., Beaufort T., Bellenger R., Berlin R., Bernardi P., Blouin D., Boumier P., Bonneau F., Briet R., Butler B., Cautain R., Chiavassa F., Costes V., Cuvilho J., Cunha-Parro V., de Oliveira Fialho F., Decaudin M., Defise J.-M., Djalal S., Docclo A., Drummond R., Dupuis O., Exil G., Fauré C., Gaboriaud A., Gamet P., Gavalda P., Grolleau E., Gueguen L., Guivarc'h V., Guterman P., Hasiba J., Huntzinger G., Hustaix H., Imbert C., Jeanville G., Johlander B., Jorda L., Journoud P., Karioty F., Kerjean L., Lafond L., Lapeyrere V., Landiech P., Larqué T., Laudet P., Le Merrer J., Leporati L., Leruyet B., Levieuge B., Llebaria A., Martin L., Mazy E., Mesnager J.-M., Michel J.-P., Moalic J.-P., Monjoin W., Naudet D., Neukirchner S., Nguyen-Kim K., Ollivier M., Orcesi J.-L., Ottacher H., Oulali A., Parisot J., Perruchot S., Piacentino A., Pinheiro da Silva L., Platzer J., Pontet B., Pradines A., Quentin C., Rohbeck U., Rolland G., Rollenhagen F., Romagnan R., Russ N., Samadi R., Schmidt R., Schwartz N., Sebbag I., Smit H., Sunter W., Tello M., Toulouse P., Ulmer B., Vandermarcq O., Vergnault E., Wallner R., Waultier G., Zanatta P., 2009, *A&A*, **506**, 411

Balona L. A., Nemec J. M., 2012, *MNRAS*, **426**, 2413

Bell K. J., Gianninas A., Hermes J. J., Winget D. E., Kilic M., Montgomery M. H., Castanheira B. G., Vanderbosch Z., Winget K. I., Brown W. R., 2017, *ApJ*, **835(2)**, 180

Bowman D. M., Kurtz D. W., Breger M., Murphy S. J., Holdsworth D. L., 2016, *MNRAS*, **460**, 1970
Bradley P. A., Guzik J. A., Miles L. F., Uytterhoeven K., Jackiewicz J., Kinemuchi K., 2015, *AJ*, **149**, 68
Brunsden E., Pollard K. R., Cottrell P. L., Uytterhoeven K., Wright D. J., De Cat P., 2015, *MNRAS*, **447**, 2970
Chapellier E., Mathias P., 2013, *A&A*, **556**, A87
Christensen-Dalsgaard J., 2008, *Ap&SS*, **316(1-4)**, 113
Córsico A. H., Althaus L. G., Miller Bertolami M. M., 2006, *A&A*, **458**, 259
Córsico A. H., Althaus L. G., Serenelli A. M., Kepler S. O., Jeffery C. S., Corti M. A., 2016, *A&A*, **588**, A74
Corti M. A., Kanaan A., Córsico A. H., Kepler S. O., Althaus L. G., Koester D., Sánchez Arias J. P., 2016, *A&A*, **587**, L5
Deleuil M., Meunier J. C., Moutou C., Surace C., Deeg H. J., Barbieri M., Debosscher J., Almenara J. M., Agneray F., Granet Y., Guterman P., Hodgkin S., 2009, *AJ*, **138(2)**, 649
Dupret M. A., Grigahcène A., Garrido R., Gabriel M., Scuflaire R., 2005, *A&A*, **435(3)**, 927
Gianninas A., Curd B., Fontaine G., Brown W. R., Kilic M., 2016, *ApJL*, **822**, L27
Grigahcène A., Antoci V., Balona L., Catanzaro G., Daszyńska-Daszkiewicz J., Guzik J. A., Handler G., Houdek G., Kurtz D. W., Marconi M., Monteiro M. J. P. F. G., Moya A., Ripepi V., Suárez J. C., Uytterhoeven K., Borucki W. J., Brown T. M., Christensen-Dalsgaard J., Gilliland R. L., Jenkins J. M., Kjeldsen H., Koch D., Bernabei S., Bradley P., Breger M., Di Criscienzo M., Dupret M. A., García R. A., García Hernández A., Jackiewicz J., Kaiser A., Lehmann H., Martín-Ruiz S., Mathias P., Molenda-Żakowicz J., Nemec J. M., Nuspl J., Paparó M., Roth M., Szabó R., Suran M. D., Ventura R., 2010, *ApJL*, **713(2)**, L192
Hermes J. J., Montgomery M. H., Gianninas A., Winget D. E., Brown W. R., Harrold S. T., Bell K. J., Kenyon S. J., Kilic M., Castanheira B. G., 2013a, *MNRAS*, **436**, 3573
Hermes J. J., Montgomery M. H., Winget D. E., Brown W. R., Gianninas A., Kilic M., Kenyon S. J., Bell K. J., Harrold S. T., 2013b, *ApJ*, **765**, 102
Hermes J. J., Montgomery M. H., Winget D. E., Brown W. R., Kilic M., Kenyon S. J., 2012, *ApJL*, **750**, L28
Kilic M., Hermes J. J., Gianninas A., Brown W. R., 2015, *MNRAS*, **446**, L26
Maxted P. F. L., Serenelli A. M., Marsh T. R., Catalán S., Mahtani D. P., Dhillon V. S., 2014, *MNRAS*, **444**, 208
Maxted P. F. L., Serenelli A. M., Miglio A., Marsh T. R., Heber U., Dhillon V. S., Littlefair S., Copperwheat C., Smalley B., Breedt E., Schaffenroth V., 2013, *Nature*, **498**, 463
Morel P., Lebreton Y., 2008, *Ap&SS*, **316**, 61
Murphy S. J., Gray R. O., Corbally C. J., Kuehn C., Bedding T. R., Killam J., 2020, *MNRAS*
Pamyatnykh A. A., 1999, *AcA*, **49**, 119
Paxton B., Bildsten L., Dotter A., Herwig F., Lesaffre P., Timmes F., 2011, *ApJS*, **192(1)**, 3
Sánchez Arias J. P., Córsico A. H., Althaus L. G., 2017, *A&A*, **597**, A29

Sánchez Arias J. P., Romero A. D., Córsico A. H., Pelisoli I., Antoci V., Kepler S. O., Althaus L. G., Corti M. A., 2018, *A&A*, **616**, A80

Serenelli A. M., Althaus L. G., Rohrmann R. D., Benvenuto O. G., 2001, *MNRAS*, **325**, 607

Tassoul M., 1980, *ApJS*, **43**, 469

Townsend R. H. D., Teitler S. A., 2013, *MNRAS*, **435**, 3406

Uytterhoeven K., Moya A., Grigahcène A., Guzik J. A., Gutiérrez-Soto J., Smalley B., Handler G., Balona L. A., Niemczura E., Fox Machado L., Benatti S., Chapellier E., Tkachenko A., Szabó R., Suárez J. C., Ripepi V., Pascual J., Mathias P., Martín-Ruíz S., Lehmann H., Jackiewicz J., Hekker S., Gruberbauer M., García R. A., Dumusque X., Díaz-Fraile D., Bradley P., Antoci V., Roth M., Leroy B., Murphy S. J., De Cat P., Cuypers J., Kjeldsen H., Christensen-Dalsgaard J., Breger M., Pigulski A., Kiss L. L., Still M., Thompson S. E., van Cleve J., 2011, *A&A*, **534**, A125